IMPROVING OBSTACLE CLIMBING WITH THE HYBRID MOBILE ROBOT OPENWHEEL i3R[1]

JEAN-CHRISTOPHE FAUROUX[†]
BELHASSEN-CHEDLI BOUZGARROU, FRÉDÉRIC CHAPELLE

Mechanical Engineering Research Group (LaMI), Blaise Pascal University Clermont -Ferrand II (UBP) and French Institute for Advanced Mechanics (IFMA), Campus de Clermont-Ferrand / Les Cézeaux, B.P. 265, 63175 AUBIERE Cedex, France

The OpenWHEEL i3R hybrid multi-mode mobile robot is introduced with a focus on its climbing mode. This wheeled robot has an articulated frame with two passive and one actuated joint that allow to climb steps through a nineteen stage sequence maintaining its static stability. This work presents a dimensional analysis of the robot climbing capacity to different design parameters such as track width, wheelbase, wheel radius, leg height, mass and mass repartition. A non symmetrical behavior during climbing is also demonstrated and justified: the front axle axle climbs easily whereas the rear axle refuses to climb. We also try to answer the difficult question of the maximum obstacle height that can be climbed for a given geometry of the robot.

1. Introduction and existing hybrid mobile robots

Locomotion systems can be defined as poly-articulated mechanical systems that interact with environment via a set of unilateral adherent or slipping contacts to the ground. These contacts may change in nature and number according to time and space [1]. Different categories of systems can be defined among which wheeled and legged mechanisms [2]. Wheels are considered to be fast and energy efficient on smooth terrain but inefficient on rough terrain. In this case, legs are more adequate and improve mobility but at the price of higher complexity of mechanical structure and control strategy.

Some robots try to take advantage both of wheels and legs and are generally named “hybrid mobile robots”. Some of them put wheels on legs such as the WorkPartner robot [3], each leg having multiple degrees of freedom. The difficulty in this case is to achieve sufficient leg stiffness and fast control. Another solution is to build an articulated frame with internal mobilities between axles. The RobuROC6 robot [4] has three axles joined by two-degree of freedom mechanisms allowing passive warping around the longitudinal axis and active rotation around the lateral axis. This is an interesting solution as the

[1] This work is supported by the TIMS research federation, Clermont-Ferrand, into the research project V2I (Intelligent Vehicles and Infrastructures).

[†] Telephone : 00.33.4.73.28.80.50. E-mail: fauroux@ifma.fr

articulated frame highly enhances the climbing capacities of the wheeled robot. Other robots rely on an entirely passive articulated frame, such as the Shrimp robot [5] that has a four-bar mounted front wheel and two pairs of lateral wheels fixed on parallelograms. This robot shows excellent climbing capacities with actuators only in the wheels (passive frame), although six wheels are required .

In this paper, we analyze the climbing capacities of the OpenWHEEL i3R robot that was first presented in [6] and tested in a reduced implementation in [7]. This robot has an articulated frame that connects the axles, similarly to RobuROC6, but with actuated warping and steering without slipping. OpenWHEEL i3R uses actuators in the wheels and only one supplemental actuator in the frame, trying to follow the simplicity rule shown by Shrimp. Contrary to these two robots, OpenWHEEL i3R uses only four wheels, an architecture that could be easily transferred to enhanced ATVs (All-Terrain Vehicles), thus giving them superior climbing capacities. OpenWHEEL i3R was first analyzed in terms of mobility and kinematics on a smooth ground in [8]. The present paper focuses mainly on the robot properties during climbing.

2. Climbing process of OpenWHEEL i3R

The kinematic structure of OpenWHEEL i3R is shown in Fig. 1. The robot is made of two axles named (A_a) with a the axle number (1 for front, 2 for rear). Wheels are numbered (W_{as}) with s the side number (1 for right, 2 for left). The axles are linked by a serial inter-axle mechanism made of two frames (F_1) and (F_2) connected by three revolute joints R_k and thus named i3R ('i' standing for "inter-axle"). Several other inter-axles mechanisms are currently under study.

The central joint R_0 is actuated and allows to lift successively each of the four wheels up to the step-obstacle, the three others serving of stable support. The R_1 and R_2 joints are passive and are used for dual Ackermann steering. They also give a longitudinal mobility that allows to bring the exploring wheel towards the obstacle (i.e. wheel W_{12} on Fig. 1). Analysis showed that the robot has a mobility of 3 while rolling and 4 while climbing [8]. Stability is ensured by permanent control of the projected center of mass G' inside the lifting triangle ($P_{11}\,P_{21}\,P_{22}$ in Fig.1). Distance HG' gives a geometric representation of the stability margin.

Each link (L) of the robot has a local reference frame $R_L\,(O_L\,,\,x_L\,,\,y_L\,,\,z_L)$. The origins O_{F1} and O_{F2} of the links (F_1) and (F_2) are defined confounded and R_{F1} represent the reference frame of the whole robot. The angles ψ, θ, ϕ represent respectively the yaw, pitch and roll of frame R_{F1} with respect to ground reference R_0. Angles θ_0 , θ_1 , θ_2 measure respectively the frame warping and axle steering of (A_1) and (A_2). They are defined by: $\theta_0=(\widehat{\boldsymbol{y}_{F1},\boldsymbol{y}_{F2}})=(\widehat{\boldsymbol{z}_{F1},\boldsymbol{z}_{F2}})$, $\theta_1=(\widehat{\boldsymbol{x}_{F1},\boldsymbol{x}_{A1}})=(\widehat{\boldsymbol{y}_{F1},\boldsymbol{y}_{A1}})$ and $\theta_2=(\widehat{\boldsymbol{x}_{F2},\boldsymbol{x}_{A2}})=(\widehat{\boldsymbol{y}_{F2},\boldsymbol{y}_{A2}})$. Only θ_0 is actuated. The steering angles θ_a are indirectly controlled via the self-rotation of the wheels θ_{as} , which are actuated, with $\theta_{as}=(\widehat{\boldsymbol{x}_{as},\boldsymbol{x}_{Aa}})=(\widehat{\boldsymbol{z}_{as},\boldsymbol{z}_{Aa}})$. The center of mass of axle (A_a) is denoted G_a and supposed located on line $(O_{Aa}, \boldsymbol{z}_{Aa})$, at the middle of the axle. This is an interesting property as it allows to steer axle (A_a) without modifying the global center of mass G, and so without affecting the stability margin.

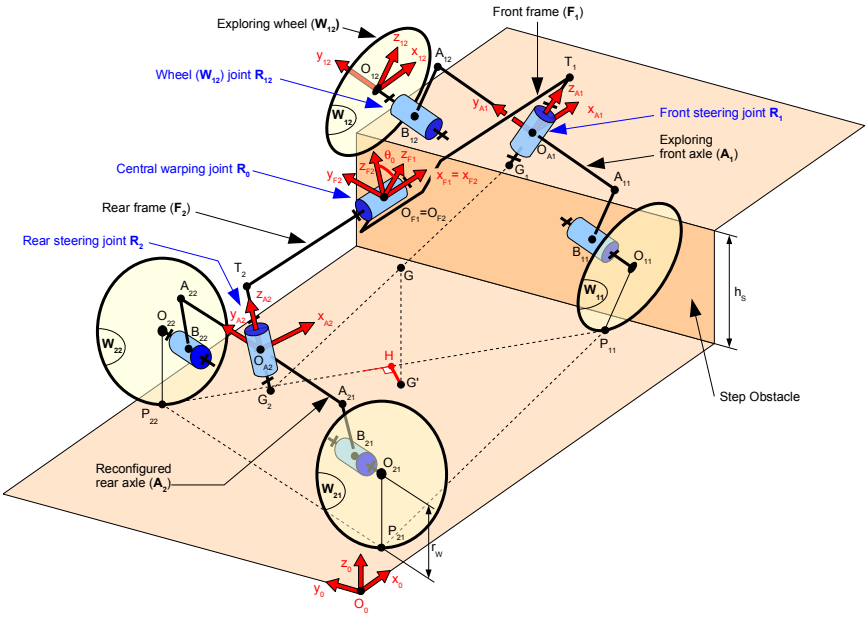

Figure 1. Kinematic structure of OpenWHEEL i3R with wheel W_{12} as an exploring wheel.

In order to climb the obstacle, each wheel has to become successively the "exploring wheel", being lifted over the obstacle while the robot lays only on three contact points P_{as}. Before lifting the exploring wheel (W_{as}), the robot must be controlled in such a way that the wheel $(W_{a's})$ of the same side s but of the other axle a' is brought as close as possible to (W_{as}). This allows to maintain G strictly above the lifting polygon (here, a triangle) and to guarantee stability.

The robot motion during climbing is described in Fig. 2. A sequence of nineteen stable key positions was presented in [7] and motion interpolation between them allows to obtain a complete process with quasi-static stability. Phase A brings the vehicle against the obstacle. In this work, the climbing process will be triggered when the robot detects the same step in front of both front wheels (W_{1s}), e.g. with ultrasonic distance sensors. Phase B is for (W_{11}) climbing. It is decomposed into four stages: stage 2 where the robot reconfigures the rear axle (A_2) to bring (W_{21}) close to (W_{11}); stage 3 where (W_{11}) is lifted via θ_0 warping; stage 4 where (W_{11}) is brought forward because of rear axle (A_2) pushing forward; stage 5 where (W_{11}) lands on top of the obstacle via via θ_0 unwarping. Phase C unrolls the same process for (W_{12}). Phase D brings the second axle in contact with the obstacle. Similarly, phase E and F are for (W_{21}) and (W_{22}) respectively. The final F phase serves only to unsteer θ_1 and θ_2.

This 2D model in top view is acceptable as a preliminary help to construct the whole climbing process. It was validated first by an Adams 3D multibody model [6] but the first experiments [7] showed it is not enough accurate with high obstacles, that mean high pitch angle and strong warping of R_0.

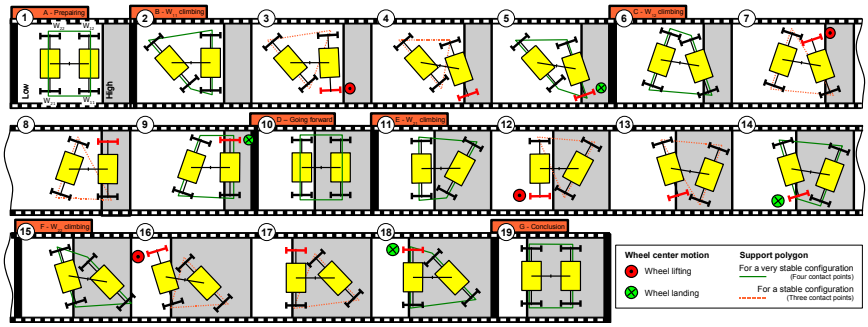

Figure 2. Climbing process of OpenWHEEL i3R in seven phases A-G and nineteen stages [7].

3. Front-rear non-symmetry

Small scale experiments have been performed on a reduced version of the robot built in Lego Mindstorms (Fig. 3a) [7]. All the lengths are modular and it is a perfect platform for testing structural solutions and validating control strategy. Control is simplified (open loop) but the robot carries its own programmable logic controller and batteries.

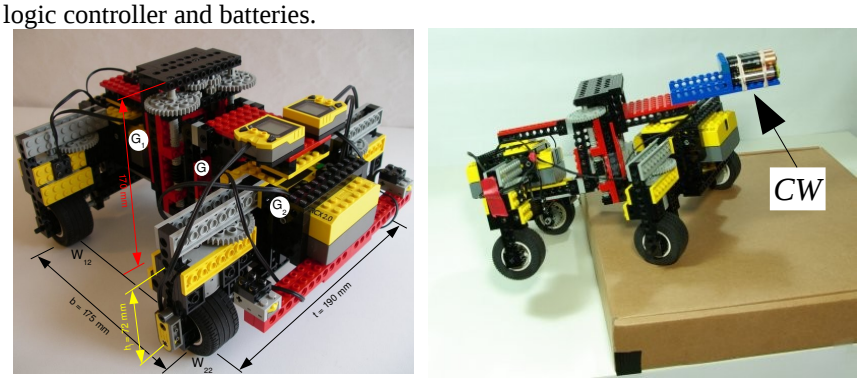

Figure 3. Small scale demonstrator of OpenWHEEL i3R (25 cm long, 1.5 kg):
(a) With dimensions (b) Climbing a 55 mm obstacle at stage 12 thanks to a counterweight *(CW)*.

Front-rear non-symmetry appeared during the tests. It was shown that axle (A_1) climbed easily the obstacle whereas axle (A_2) was blocked. The adopted solution was to use a counterweight *(CW)* in front of (A_1) to move the center of mass G of 16mm forward (9% of the wheelbase) and re-equilibrate the front-rear behavior (Fig. 3b). At this condition, the best climbing test allowed to climb a step as high as 67% of the altitude of the center of mass.

The non-symmetry was not predicted in Fig. 2 because of the 2D approximation. On flat ground (Fig. 4a), the 2D model is exact. When the pitch angle θ grows, the 2D model becomes approximate because distance P_2G' is evaluated as $b\cos(\theta)/2$ (Fig. 4b). In reality, the projected center of mass G' is located more on the left because of leg height h_l and P_2G' is $-h_l\sin(\theta)+b\cos(\theta)/2$ that can be also written $-h_l h_s/b+b\cos(\theta)/2$ (Fig. 4c). This discrepancy favors stability at stages 3 and 7 and penalizes stability at stages 12

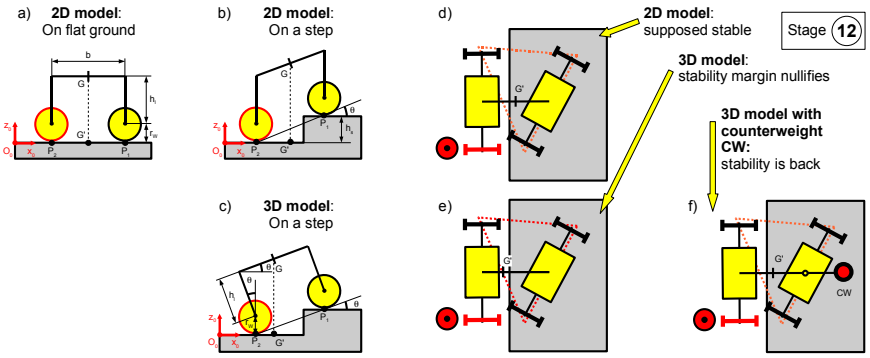

Figure 4. Modelling the front-rear non-symmetry on stage 12.

and 16. If we take the example of stage 12 (Fig. 4d), G' is located 23 mm at the rear of its expected position, which nullifies the stability margin and prevents the rear axle to climb (Fig. 4e). Putting a counterweight CW allows to shift forward the center of mass and to equilibrate the climbing capacities of front and rear axles (Fig. 4f).

4. Dimensional analysis of several design parameters

Another interesting point is to understand the effect of the dimensional parameters of the robot on its climbing behavior on a step of height h_S. The considered parameters in this work are track width, wheelbase, wheel radius, leg height, mass and mass repartition.

Track width *t* is defined by $O_{a1}O_{a2}$, distance between the centers of the wheels on a same axle. The climbing capacity h_{Max} of the exploring wheel must be higher than obstacle height h_S and can be approximated, in projection in the (O_0, y_0, z_0) plane, to $h_{Max} = t \sin(\theta_{0\,Max})$ (Fig. 5a). When t increases, h_{Max} increases proportionnally. $\theta_{0\,Max}$ is kept around 45° in absolute value to avoid tire roll-off. This means a lower bound for t can be expressed by $t_{Min} = h_S / \sin(\theta_{0\,Max})$.

For its maximum value, t is bounded by the risk of collision between wheels of the same side during double steering (Fig. 5b). The maximal steering angles $\theta_{a\,Max}$ are evaluated around 45° to stay away from the singular configuration where all the contact points P_{as} are aligned, which is laterally

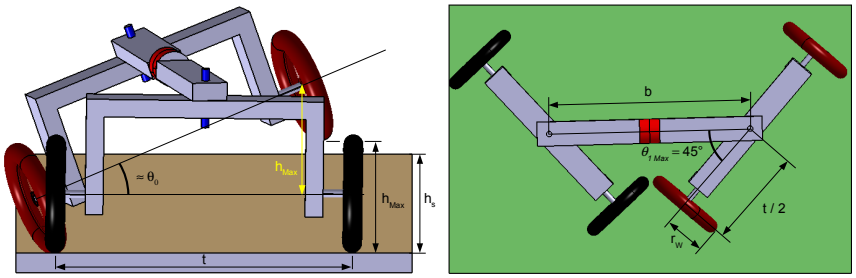

Figure 5. Evaluating the bounds for (a) t_{Min} (b) t_{Max}.

unstable. The closure condition when there is contact between the wheels gives $t_{Max} = (b - 2r_W \sin(\theta_{\alpha Max})) / \cos(\theta_{\alpha Max})$.

Wheelbase *b* is the length T_1T_2 . There is a minimum value of *b* that allows to avoid collision of the axles during double steering. The calculation are developed above in the track width section.

There is no precise upper limit to *b* apart the fact that a long robot may become heavy and difficult to steer. It should be noted that a long robot takes less pitch during climbing and is less sensitive to front-rear non-symmetry. A practical limit could be $b_{Max} = 2.t$.

Wheel radius r_W : it should be sufficiently big to roll correctly on irregular terrain. It is commonly admitted that a small obstacle of height h_o will be crossable by a wheel of radius $r_W = 4.h_o$ (example of a bike on a pavement side). Even with extra-small wheels, the robot is able to climb big steps (Fig. 6a). This means the robot relies on its frame and not on its wheels for step climbing. Wheels are only here to roll. Climbing performance should be measured by comparing the obstacle height with the center of gravity, not the wheel diameter.

If r_W increases too much, there is a risk of collision between wheels. The exploring wheel has a longer longitudinal travel along x_0 to go above the obstacle. In the configuration where (W_{12}) is blocked between the wall and (F_1) while (W_{11}) is exploring the step (Fig. 6b), an upper bound on r_W is simply $t/2$.

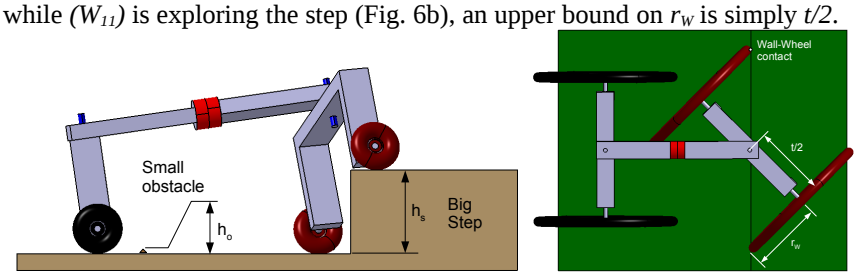

Figure 6. Evaluating the bounds for r_w : (a) wheels can be very small (b) the biggest wheels.

Leg height h_l represents length $A_{as}B_{as}$. With a null value of h_l, collision occurs between the axle of the exploring wheel and the edge of the step (Fig. 7a). Having a minimum value is compulsory (Fig. 7b). Collision can be avoided if $r_W + h_l \geq h_s$, which gives the lower bound $h_{lMin} = h_s - r_W$.

If h_l becomes too big, the front-rear non-symmetry phenomenon intensifies, which is penalizing for the overall behavior. One can suggest that $r_W + h_l \leq 2h_s$, which gives the upper bound $h_{lMax} = 2h_s - r_W$.

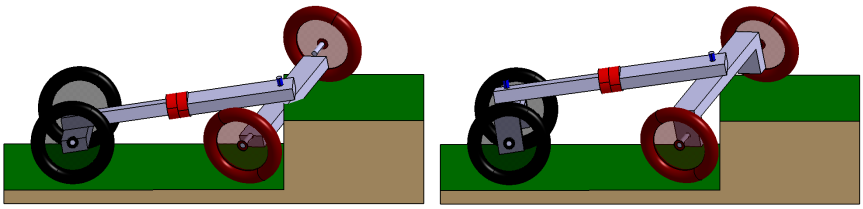

Figure 7. Evaluating the bounds for h_l : (a) collision with null value of h_l (b) longer leg.

Mass: the climbing process requires friction tangential forces T on the ground such that $T < \mu N$ with μ the friction coefficient and N the normal force. When the mass increases, N and T increase proportionally. This means mass is not a significant parameter on hard grounds. The limit value of T corresponds to the maximum obstacle height that can be climbed with these adherence conditions. This changes on granular terrains where the Coulomb friction model cannot be applied. A too heavy robot may also dig ruts on the track.

Mass repartition: lateral symmetry with respect to plane (O_{F1}, x_{F1}, z_{F1}) guarantees identical left and right behaviors. Longitudinal symmetry with respect to plane (O_{F1}, y_{F1}, z_{F1}) must be broken to equilibrate the climbing capacities of the front and rear axles (cf. §3). Solutions include adding a frontal counterweight, modifying mass repartition or changing geometry on one axle.

Maximal obstacle height: An interesting question is to determine the maximum value of the step height h_S that such a robot with given dimensions can climb. The critical stages where climbing was at the limit of stability were stages 4, 8, 13 and 17 (the third stages of each phase). A precise answer requires a complete stability analysis for each stage and must start by solving the direct geometric problem of the robot, that can be considered as a parallel mechanism. A rough approximation is $h_{Max} = t \sin(\theta_{0Max})$ but this value is penalized by several phenomena, e.g. the decrease of the altitude of the exploring wheel when brought forward and the potential loss of adherence of some supporting wheels.

5. Towards a full scale experiment

Table 1 summarizes the lower and upper bounds on each main parameter of the robot. The parameters are put in the logical order of selection. The first is track width t, that is tightly connected with obstacle height h_S. The second is wheel radius r_W. From both parameters, one can derive wheelbase b and leg height h_l.

Table 1. Bound values of the main design parameters (the bound values of $\theta_0, \theta_1, \theta_2$ are set to 45°).

Parameter	Name	Lower bound	Upper bound
Track width	t	$t_{Min} = h_S\sqrt{2}$	$t_{Max} = b\sqrt{2} - 2r_W$
Wheel radius	r_W	$r_{WMin} = 4\,h_O$	$r_{WMax} = t/2$
Wheelbase	b	$b_{Min} = \sqrt{2}(t/2 + r_W)$	$b_{Max} = 2.t$
Leg height	h_l	$h_{lMin} = h_s - r_W$	$h_{lMax} = 2\,h_s - r_W$

From these equations are drawn the dimensions of the bigger prototype of OpenWHEEL i3R which is under construction (Fig. 8). The frame is made of modular aluminium profiles that can be easily adjusted in length according to the experiments.

The robot has t = 1.2 m, r_w = 0.2 m and weighs around 150 kg. It is actuated by five DC moto-reducers (330 W each, nominal torque 30 Nm, peak torque 100 Nm during a few minutes). This platform will be easy to enrich with supplemental sensors such as obstacle detection devices, angular encoders on the steering axles, force plates inside wheel hubs. An automatic inflation system is also planned for dynamic adjustment of the wheel tangential force.

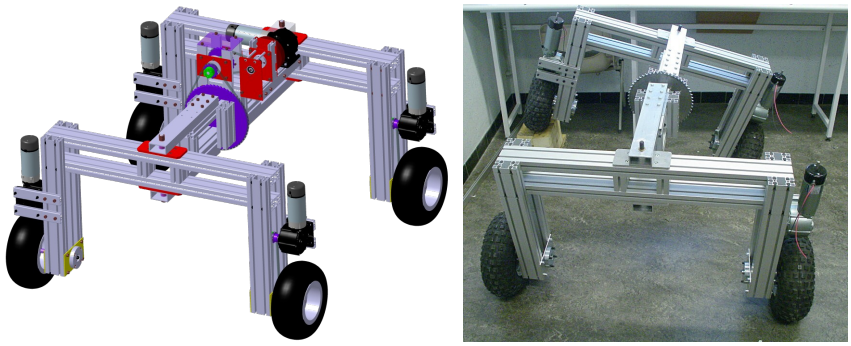

Figure 8. Full scale demonstrator of OpenWHEEL i3R (t = 1.2 m, r_w = 0.2 m, 150 kg). (a) CAD model (b) Preliminary assembly of the full scale model [9].

6. Conclusion

This work presented a dimensional analysis of the main parameters of the OpenWHEEL i3R hybrid mobile robot and their effect on the obstacle-climbing mode. It also permitted to define design rules for building a customized robot according to the obstacles to be climbed. A phenomenon named "front-rear non-symmetry", that penalizes only the rear axle during climbing, was presented and justified, as well as the height of the maximum obstacles that can be climbed for a given geometry. Experimental results on a small scale robot confirm the analysis. The full scale version of the robot, including supplemental sensors, gives an idea of the climbing capacities that most ATVs will have in the future.

References

1. F. Ben Amar, P. Bidaud, S. Barthélémy and C. Grand, "Mobilité et stabilité des systèmes à roues et/ou pattes". Proc. of Journées Nationales de Recherche en Robotique JNRR'2007, 9-12 oct. 2007, Strasbourg. http://jnrr07.u-strasbg.fr/actes/articles/13.pdf.
2. M.G. Bekker, *Introduction to terrain-vehicle systems*. The University of Michigan Press, 1969.
3. A. Halme, I. Leppänen, J. Suomela, S. Ylönen and I. Kettunen, "WorkPartner: interactive human-like service robot for outdoor applications", *International Journal of Robotics Research*, vol. 22, no 7-8, pp. 627-640 (2003).
4. Robosoft, *MiniROC/RobuROC6 mobile platform*, http://www.robosoft.com/eng/, http://www.robosoft.fr/img/data/robuROC6_web1.pdf (2009).
5. T. Estier, Y. Crausaz, B. Merminod, M. Lauria, R.Piguet and R. Siegwart, "An innovative Space Rover with Extended Climbing Alilities", Proceedings of Space and Robotics 2000, Albuquerque, USA, Feb. 27-March 2 (2000).
6. J.C. Fauroux, B.C. Bouzgarrou and F. Chapelle, "A New Principle for Climbing Wheeled Robots: Serpentine Climbing with the OpenWHEEL Platform", Proc. of IEEE/RSJ Int. Conf. on Intelligent Robot and Systems, IROS'2006, Beijing, China, October 9-15, 2006, pp.3405-3410, file IROS06-553.pdf.
7. J.C. Fauroux, B.C. Bouzgarrou and F. Chapelle, "Experimental validation of stable obstacle climbing with a four-wheel mobile robot OpenWHEEL i3R", in Proc. 10th International Conference on Mechanisms and Mechanical Transmissions, MTM'2008, October 8-10, 2008, Timisoara, Romania, 8p.
8. B.C. Bouzgarrou, F. Chapelle and J.C. Fauroux, "Preliminary Design and Analysis of the Mobile Robot OpenWHEEL i3R", in Proc. 3rd 1.Third International Congress Design and Modelling of Mechanical Systems, CMSM'2009, March 16-18, 2009, Hammamet, Tunisia, 8p.
9. L. Genevay, "Assembly and control of OpenWHEEL i3R", IFMA final year project (2009).